33RD CONGRESS
OF THE INTERNATIONAL COUNCIL
OF THE AERONAUTICAL SCIENCES
STOCKHOLM, SWEDEN, 4-9 SEPTEMBER, 2022

ICAS 2022 SWEDEN

EVALUATION ENVIRONMENT FOR CASCADED AND PARTLY DECENTRALIZED MULTI-RATE LOAD ALLEVIATION CONTROLLERS

Christian Wallace[1], Simon Schulz[2], Nicolas Fezans[1], Thiemo Kier[2] & Guido Weber[3]

[1]DLR, Institute of Flight Systems, Lilienthalplatz 7, 38108 Braunschweig, Germany
[2]DLR, Institute of System Dynamics and Control, Münchener Str. 20, 82234 Wessling, Germany
[3]Liebherr-Aerospace Lindenberg GmbH, Pfänderstr. 50-52, 88161 Lindenberg, Germany

Abstract

This paper presents a simulation environment to evaluate the load alleviation performance of partly decentralized and multi-rate load alleviation control structures. The environment is implemented in MATLAB® and Simulink® and includes several parts written in C++. The proposed control architecture targets all types of EASA CS 25 / FAR Part 25 aircraft. In this work, the application to a Generic Long Range Aircraft research model is considered. The architecture includes new sensor technologies and related load control functions, like a lidar-based feedforward control loop, centralized *rigid-body* and flexible control laws as well as fast local feedback control loops, enabling quasi-immediate reaction of the wing to external disturbances. The features of the simulation environment are discussed in detail along with this controller structure and the considered aircraft model.

Keywords: Gust load alleviation, evaluation environment, cascaded and decentralized controllers, lidar

1. Introduction

Due to the global warming and the climate change, society's expectations and goals for a future clean and sustainable civil aviation are ambitious. In addition to the direct improvement of engine efficiency or the use of sustainable aviation fuel (SAF), the reduction of the aircraft net weight in order to reduce induced drag and therefore the power or fuel consumption has always been an essential research objective in aeronautics. The design of the structural layout for the wings is mostly driven by inertia and aerodynamic loads. Airplanes in operational service are inevitably exposed to manifold loads during different flight phases. Beside the landing and maneuvering loads, the airplane is also subject to external disturbances like turbulence and gusts.

Even if other load types cannot be ignored and if manufacturing constraints may impose minimum thicknesses on some parts, significant portions of the primary wing root structure of typical modern CS 25 aircraft are often sized by gust load cases, particularly if a maneuver load alleviation (MLA) function has been already taken into account. Hence, the difference between the gust load envelope and the next type of loads is usually the load alleviation target that gust load alleviation (GLA) systems could help converting into weight savings.

Active gust load alleviation is providing the opportunity to exploit potentials to modify and redistribute the wing lift distribution to lower structural loads dynamically, ideally considering the dynamic behavior of the flexible structure. Common load alleviation strategies are based on sensor technologies like the centralized inertial measurement unit (IMU) or distributed acceleration measurements on the airframe [1], both processed by a central feedback controller. Beyond that, a significantly improved gust load alleviation performance can probably be expected by using more complex/advanced control

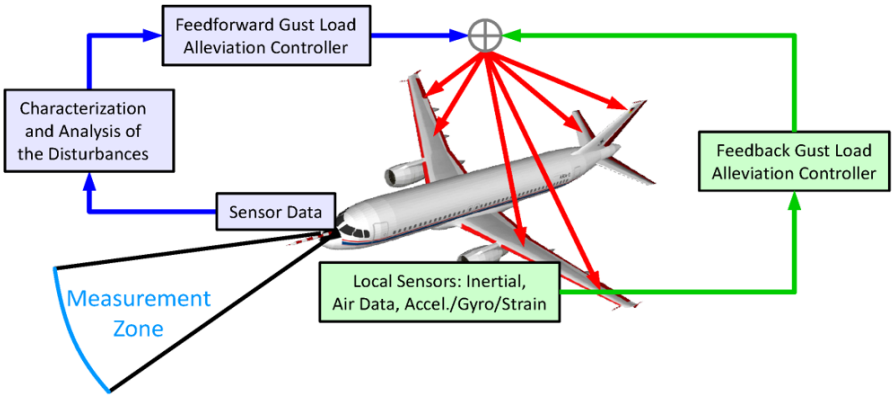

Figure 1 – Schematic illustration of lidar-based feedforward control in combination with feedback gust load alleviation

architectures and systems, like feedforward controller structures using lidar-based measurement signals of the encountered disturbance [2–5] or fast and decentralized feedback load alleviation control loops [6].

Within the framework of the German national research project INTELWI, numerous partners are developing novel control approaches, devices, and simulation tools and applying them to a couple of representative aircraft configurations. To support the joint work of DLR and Liebherr on partly decentralized control architectures, a common simulation and evaluation environment for the Generic Long Range Aircraft (GLRA) configuration is developed. The considered decentralized controller architecture includes a baseline rigid-body controller, a feedforward-based gust load alleviation function as well as centralized and decentralized / local feedback alleviation controllers. The decentralized / local and fast feedback controller loops considered rely on so-called Remote Electronic Units (REU).

The investigation of load alleviation capabilities of novel technology approaches can be a challenging task and a therefore time-consuming process. Especially, if not only a single approach is investigated solely, but different combined techniques should be analyzed. Hence, the successful application of complex load alleviation structures requires efficient, flexible and versatile development tools that enables the controller designer to get an in-depth look into the overall system behavior as well as in the interaction of sub-parts. The upcoming section 2.provides an overview of the novel load alleviation techniques to be investigated as well as previous work on these technologies. Section 3.presents the overall (and prospective) controller architecture, supplemented by a description of the used GLRA model. Section 4. details the key features of the simulation environment and the way it is integrated in the overall process of load evaluation.

2. Novel Active Load Alleviation Technologies and Previous Research Activities

In contrast to a feedback gust load alleviation controller that uses different sensors on the airframe, which measure the aircraft response during a gust encounter, significantly higher load alleviation performance can be achieved by using optical lidar sensors to detect the atmospheric disturbances in advance. For this, a measurement zone ahead of the airplane is scanned (see Figure 1). The measured data is processed afterwards by a windfield estimation algorithm which interprets the lidar raw Line of Sight (LoS) speed measurements to extract detailed information of the upcoming windfield. The feedforward GLA controller function can then leverage the wind information to start taking control actions before changes in the aerodynamic loads occur. That enables, for instance, to adjust the motion (trajectory) of the aircraft through pitching commands, allowing alleviating the angle-of-attack variations induced by the gust. A dynamic redistribution of the lift along the wing can also be performed simultaneously; considering the gust-induced aerodynamic response (including unsteady aerodynamic effects); the superimposed pitching motions that would result from the gust encounter and from the controller actions; the frequency response of the structure. Hence, a prepared airplane is flying (in anticipation of) the disturbance through the windfield, ensuring a lowered level of loads.

In recent years, various aspects linked to lidar-based gust load alleviation systems have been investigated by the authors [7–9]. The presented concepts are characterized by modern robust controller synthesis methods in combination with a gust disturbance feedforward controller. The reader is referred to the literature for an overview on lidar sensor technology and its possible use for gust load alleviation [10, 11] and for the on-going wind lidar developments for aeronautical applications at DLR [12–14]. Reconstruction techniques need to be used to determine the wind field ahead of the aircraft based on the lidar measurements. DLR proposed optimized versions of these algorithms for the gust load alleviation use case [8, 15]. A controller synthesis approach was specially optimized for the design of lidar-based gust load alleviation functions. It was tested and demonstrated first on a fairly simple flexible model of the DLR Discus-2c sailplane [3, 16, 17] and recently scaled-up and integrated into a comprehensive methodology that can be applied to industrially-relevant configurations [9]. The evaluation environment presented in this paper is an evolution of the multi-rate hybrid simulation environment developed for the work presented in [9]. In the INTELWI project, a further *scale-up* is being made by considering even more flight points, mass configurations, and load stations (for a different aircraft) as well as more complex actuator and sensor models.

Apart from the investigation of the use of lidar sensors for gust load alleviation, the advantages of using a multi-rate decentralized control architecture is investigated in cooperation between DLR and Liebherr. The idea is to allow high-bandwidth local control loops with local sensors being used to compute additional feedback commands to the neighboring actuators. Such loops could operate with higher sampling rate (e.g., between 300 and 1000 Hz) and less delay.

3. Description of the Used Aircraft Model and the Investigated Controller Architecture

3.1 Flexible Aircraft Model

The GLRA is modeled using the framework VarLoads [18]. This modeling approach has been used for multiple applications from loads analysis of whole flight missions [19], to multiple applications for gust load alleviation [20], primary flight control design for high altitude platforms [21], loads analysis with complex wind-fields like wake vortex encounters [22] and evaluation of newly introduced load conditions in the CS-25 [23].

In VarLoads, the structural stiffness is represented by a finite element model, which is statically reduced to component-based loads reference axes as proposed by Guyan in [24]. Since only the primary structure is included in the finite element model, the masses are usually not obtained from material density. Typically, a database-driven approach is employed to obtain the operating empty weight of the aircraft including systems, secondary structure and equipment. Additionally, several payload/fuel combinations are generated to cover enough (according to CS 25.321 in [25]) combinations of positions of center of gravity and weights. These masses are then attached to the reduced model and a modal analysis is carried out. The equations of motion are based on the so called “mean axes” formulation [26], resulting in non-linear Newton-Euler equations of motion for the rigid body and a linear modal representation of structural dynamics:

$$\begin{aligned} \begin{bmatrix} m_b \left(\dot{V}_b + \Omega_b \times V_b - T_{bE}\, g_E \right) \\ J_b\, \dot{\Omega}_b + \Omega_b \times (J_b\, \Omega_b) \end{bmatrix} &= \Phi_{gb}^T\, P_g^{ext} \\ M_{ff}\, \ddot{u}_f + B_{ff}\, \dot{u}_f + K_{ff}\, u_f &= \Phi_{gf}^T\, P_g^{ext}. \end{aligned} \tag{1}$$

V_b is representing the velocity and Ω_b is representing the angular velocity Ω_b of the structure, both expressed in the *body* reference system. The total mass is defined by m_b with the corresponding inertia tensor J_b. The matrices Φ_{gb}, Φ_{gf} are the modal transformation matrices. The matrices M_{ff}, B_{ff} and K_{ff} describe the modal mass, damping and stiffness matrix and u is describing the modal deformation vector. The external loads P_g^{ext}, are mainly caused by the aerodynamics and the propulsion. The aerodynamic loads are derived by applying an unsteady panel method based on potential flow theory, namely the doublet lattice method (DLM). The DLM calculates the aerodynamic matrices at discrete reduced frequencies. To use this data for time domain simulations a so-called rational function approximation (RFA) is used, which allows the unsteady aerodynamic model to be cast in state space

form. The integrated or cut loads are recovered by the so called force summation method (FSM) [27]. The model also provides flight mechanical parameters like position, velocities, angular rates and aerodynamic sensor data consisting of angle-of-attack and angle-of-sideslip. Distributed acceleration and rotation rates at various locations of the flexible structure provide essential information required by flight control laws. Aerodynamic hinge moments are calculated for every control surface as inputs for the actuator models. For more detailed information about the modeling approach, the reader is referred to [28].

Currently, nine different mass distributions, in combination with three altitudes and one design speed V_c (see CS 25.335 in [25]) are available, for the clean configuration (only the stabilizer has a trim value unequal to zero) as well as for the air-brake-out configuration. Altogether, two flight conditions are approximated by nearly 110 different linear time-invariant (LTI) models. Every LTI model has 36 inputs for the control surfaces: i.a. eight different ailerons, two winglet tabs, six flaps, and a total of 12 spoilers. To excite the aircraft via gusts and turbulent wind fields 50 different planes/zones perpendicular to the fuselage axis and distributed along the longitudinal aircraft axes are defined. The normalized vertical wind velocity (normalized by dividing it with the true airspeed) and its time-derivative are required for each zone. This results in 100 wind inputs in total. The structural model contains over 400 distributed structural points to monitor cut loads, resulting in over 2500 cut load outputs (3 forces and 3 moments for each point) over the overall aircraft structure. 32 outputs provide the hinge moments (needed for considering the load on the actuators). Over 4800 outputs are used for structural velocities and accelerations. The aeroelastic model has about 2800 states.

In the following, only symmetrical load cases are considered (wings level, no sideslip, no lateral gust).

3.2 Considered Controller Architecture

The controller architectures investigated in the INTELWI project consist of combinations of centralized control functions and of fast and decentralized local loops, cf. Figure 2. In this figure, all centralized control functions are gathered in the light orange box, which symbolizes the flight control computer (FCC). The FCC is usually installed in the avionics bay close to the cockpit. The “local loops” involve so-called Remote Electronic Units (REU) and actuators, represented in Figure 2 by the light and dark gray boxes, respectively. The following subsections present the different centralized control functions as well as the REU and the decentralized control function that runs on them.

3.2.1 Baseline Controller

An Airbus-like representative baseline “rigid-body” controller is included in the central FCC. Whilst all autopilot vertical modes could be considered and especially the ones that are active for extensive period of times, a manual C* pitch law [29, 30] was chosen. It contains both a pilot input feedforward shaping filter and a fairly classical PID-like feedback structure. The feedback part was tuned as a compromise between low feedback gains, robustness to model uncertainties, and disturbance rejection. The controller increases the damping of the short period mode and marginally modify its frequency. The integral term ensures the compensation of model static errors but, thanks to adequate feedforward gains and filters, is not used for reference tracking on the “nominal” system. The remaining degrees of freedom of pilot input feedforward filter are tuned to provide a stick input response fairly well-centered within the C* upper and lower limits [29]. Such control functions are known to suppress the speed stability (i.e., the stability of the phugoid mode), however the slow drift in speed that could result from it is easy to control by the pilots and is too slow to impact the peak gust loads obtained for discrete gust encounters as specified in paragraph 25.341a of the CS-25 [25]. This controller only acts on the elevator commands.

Such function is typically implemented in a partition of the flight control computer running at 25 Hz (i.e., 40 ms sampling time). It is normally tuned with fairly low gains and there is usually no significant difference between the results obtained with a 25 Hz discrete-time implementation and with its simulation as continuous-time system. Nevertheless, this baseline controller can and will to some extent measure the consequences of the encountered gust and turbulence, through the sensor measurements (e.g., n_z, q) used in its feedback path. It will react to these measurements, already impact the

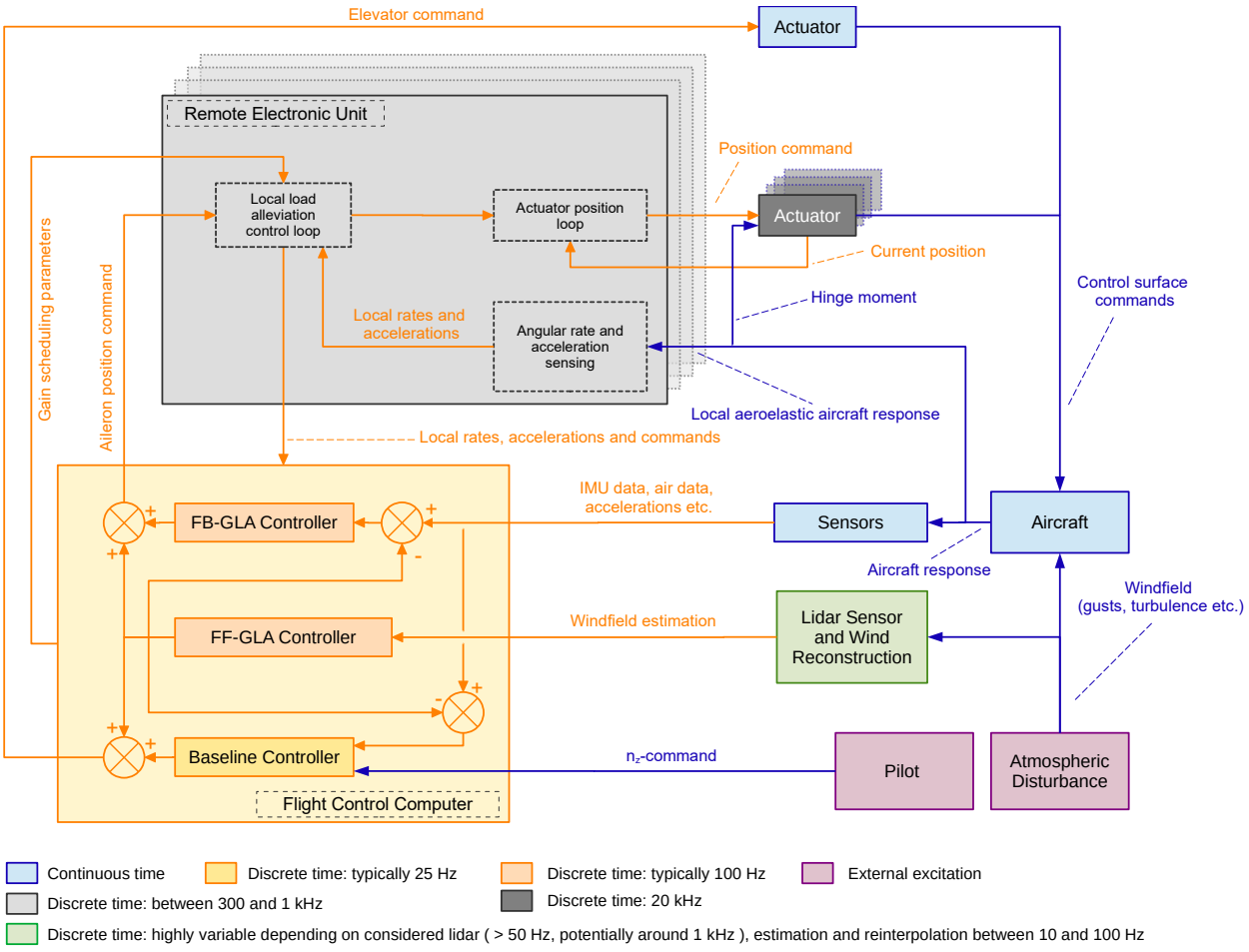

Figure 2 – Partly decentralized load alleviation control approach including Remote Electronic Units for aileron surface control (FF-GLA: Feedforward Gust Load Alleviation, FB-GLA: Feedback Gust Load Alleviation)

gust loads, and possibly interact with the other control functions, which is why it should be considered in the evaluation model.

3.2.2 Feedback GLA Controller

Feedback gust load alleviation (FB-GLA) controllers (typically implemented in discrete time at 100 Hz) use measurements from the inertial reference system and, possibly, angle-of-attack measurements as well as other measurements across the aircraft (e.g., local accelerations or rotational rates). Their tuning may be performed in many different ways, but a FB-GLA controller's role is typically to control structural loads while not affecting the handling qualities. In comparison to a baseline functionality, these types of controllers will be active in a slightly higher frequency range which will be typically restricted to a band of about 1 to 4 Hz. These values depend on the frequency of the aircraft modes. The lower bound is constrained by the desire to not affect the handling qualities and is therefore relatively constant for all CS-25 airplanes. The definition of the upper bound is less clear, above 4-5 Hz the terms "vibration control" might be employed and there might be a dedicated vibration control function. In other cases, the same FB-GLA controller might also be active at higher frequencies. The FB-GLA function usually contains a roll-off behavior to prevent transmission of measurement noise and is designed such that no constant deflections can be commanded on any of the control surfaces.

3.2.3 Lidar-Based Feedforward GLA Controller

A lidar-based feedforward gust load alleviation function is also included. It consists of a Doppler lidar sensor, post-processing algorithms allowing the interpretation of the LoS lidar measurements (wind

reconstruction), and a preview controller that exploits the obtained near-future wind information to optimize the aircraft response and reduce the loads induced by gust and turbulence. Compared to those obtained from more classical air data sensors, the lidar-based wind measurements are neither particularly precise nor well capturing the higher frequencies of the disturbances (above 4-5 Hz). For a frequency-based analysis of the wind information that can be extracted from Doppler lidar measurements, the reader is referred to [8].

Getting wind information through the lidar wind measurements ahead of the aircraft slightly in advance (by typically 0.3 s to 0.6 s) allows using (elevator) pitching commands, in addition to commands to the ailerons and spoilers. Changing the angle of attack is extremely effective and efficient for modulating the aerodynamic forces, but very limited in terms of control bandwidth. Only very low frequency pitching commands can be used in practice due to the limited deflection rates of the elevators, to the horizontal tailplane (HTP) and fuselage loads, and to comfort considerations for passengers at the front and at the aft of the cabin. Further information on the design of preview controllers for lidar-based gust load alleviation can be found in [5, 9, 31] and references therein. As the feedforward controller anticipate the upcoming disturbances, the result of its actions may be detected by the feedback control functions (baseline controller and FB-GLA controller). To prevent them from counteracting the actions of the feedforward GLA controller (FF-GLA), further outputs from the FF-GLA are used to "correct" the sensor measurements used by the feedback controllers (cf. Figure 2).

3.2.4 Decentralized Fast Local Alleviation Loops

As shown in Figure 2 (gray boxes), Remote Electronic Units are used to implement fast decentralized local alleviation loops. The REU can be thought as a small-size ruggedized embedded control computer which also contains a three-axis accelerometer and a three-axis gyrometer. It can operate in severe environment (unpressurized area with high vibration levels and cold soak). It can be used to control the local actuators and to process data (concentration, monitoring, conversion). It fulfills design assurance level (DAL) A, is RTCA/DO-160 qualified and is developed according to RTCA/DO-178C and DO-254. It provides two independent and dissimilar computing lanes. The dynamic response of the REU and its sensors to physical accelerations is being characterized in [6]. The sensor dynamic models are presently in development and will be implemented to the simulation environment presented later when available.

By using the local acceleration and rotational rate measurements to compute additional control commands for the aileron(s) located in the direct vicinity of the REU, the overall delay in these local loops can be brought to very low values. The local functions can be implemented in discrete time with higher sampling rate than typically done in the centralized flight control computer (300 Hz to 1 kHz vs. typically 100 Hz in the FCC). This eases the implementation of fairly high-bandwidth controllers, which might be very advantageous for alleviating fairly short gusts (possibly sizing for the outer part of the wing and the winglet) or for active flutter suppression.

4. Environment(s) for the evaluation of the load alleviation performance

This section presents various environments, denoted by different degrees of complexity, which enables to perform more or less detailed analysis of the load alleviation performance. To understand the origins and differences between these environments and the models they are based on, section 4.1 presents the controller design process (including model transformations, reductions, etc.), the different models being generated at different steps, and the way these models and derived versions of these models can be used for quick assessment of the controller performances. Later, section 4.2 presents a significantly more advanced simulation environment, with which more realistic models of the flight control architecture and its components are used. This environment is more demanding but more powerful and more precise. It is often used as a reference for the authors' load alleviation studies, to assess the performance of the controllers that are found promising using the faster, yet less precise, performance evaluations.

4.1 Data and model flow during controller design and related linear evaluation environments

4.1.1 Model transformations during controller design

The model transformations made during the design of the lidar-based feedforward gust load alleviation function lead to the flow diagram shown in the left part of Figure 3. In that case, the original continuous-time full-order models (CT **F**OM) are transformed and simplified in several steps, yielding the continuous-time reduced-order model (CT **R**OM). This model is then discretized (DT **R**OM). Eventually, the model is augmented by a chain of unit delays (or tapped delay-line) on the previewed inputs, some of its transfers are normalized, and possibly weighted to obtain a standard control synthesis problem on which the synthesis is made in discrete time. For simplicity, the present explanation only considers the different models linked to the lidar-based feedforward/preview control gust load alleviation function. Other models may be generated during the design of the feedback gust load alleviation controller and these models could also be considered in the following. The exact steps followed and the variants of the models being generated mainly depends on a) the control design methodology used and b) the properties and format of the original model and the considered subsystems.

Depending on the way the model was built and structured, various processing steps might be required. Some models are built with different zones with separate wind inputs for each zone, others directly include lag effects/states to account for the time delay between the gust encounter on the nose of the airplane, on the wings, and on the HTP. Some aeroelastic tools produce models with separate inputs for wind/control surface deflections and their time-derivatives (possibly several of them). The transformations may involve using Padé approximants [32] (or similar) to account for time delays, or using pseudo-differentiator filters (e.g., $s/(\varepsilon s+1)$ with ε small) to replace inputs that are time-derivatives of each other with a single equivalent input. The steps and different model variants explained in Figure 3 should therefore be understood as an illustration based on a specific example.

The aero(servo)elastic models used are typically based on a modal formulation of the structure (originated from a finite element discretization) and coupled with an (unsteady) aerodynamics model. This typically leads to models having between a few hundred and a few thousand states, which also include quite high-frequency modes (with significantly higher frequencies than those of interest for gust load alleviation). For a reduced computational effort and numerical robustness reasons a model reduction step is usually required prior to the synthesis, transforming a full-order model into a reduced-order model. If several controllers are tuned, various levels of reductions might be used for each controller synthesis as the requirements may differ (not represented in Figure 3).

Quite often, the controller design is done on a continuous-time model and the controller is discretized afterwards. The preview control approach used to design the lidar-based feedforward controller is easier to express as a discrete-time control synthesis problem because the gained wind information is a piece of the wind profile ahead of the aircraft, as schematically represented in Figure 4a. The (vertical) wind profile in blue is discretized for the positions at which the aircraft is now, will be in 1, 2, ..., h timesteps. In discrete time, this can easily be represented by the h unit delays located prior to the wind input of the aircraft model, cf. Figure 4b. They constitute a tapped delay-line with the left-most element d_p corresponding to the left-most red dot in Figure 4a. The subsequent elements of the series of red dots in Figure 4a and of the tapped delay-line in Figure 4b are equivalent. On a side note, each row of the input (B) matrix of the controller $K(z)$ contains gains related to the feedback signals y_{FB} (if any) and a series of coefficients with which the tapped values are multiplied. The combination of this series of coefficients and the tapped delay-line constitute a finite impulse response filter (FIR). Whilst, this interpretation as FIR is not truly required for understanding the various evaluation environments, it explains why the preview control approach is used and why, among other things, a chain of unit delays is added to the (DT **R**OM) when building the control design model in the lower-left part of Figure 3.

4.1.2 Performance evaluation based on the available model variants

The controller design process (left side of the diagram of Figure 3) involves several steps of model processing, augmentation, simplification, etc. Not all of these models are directly suited for validation as illustrated on the right side of this figure. The simplest validation is to use directly the designed con-

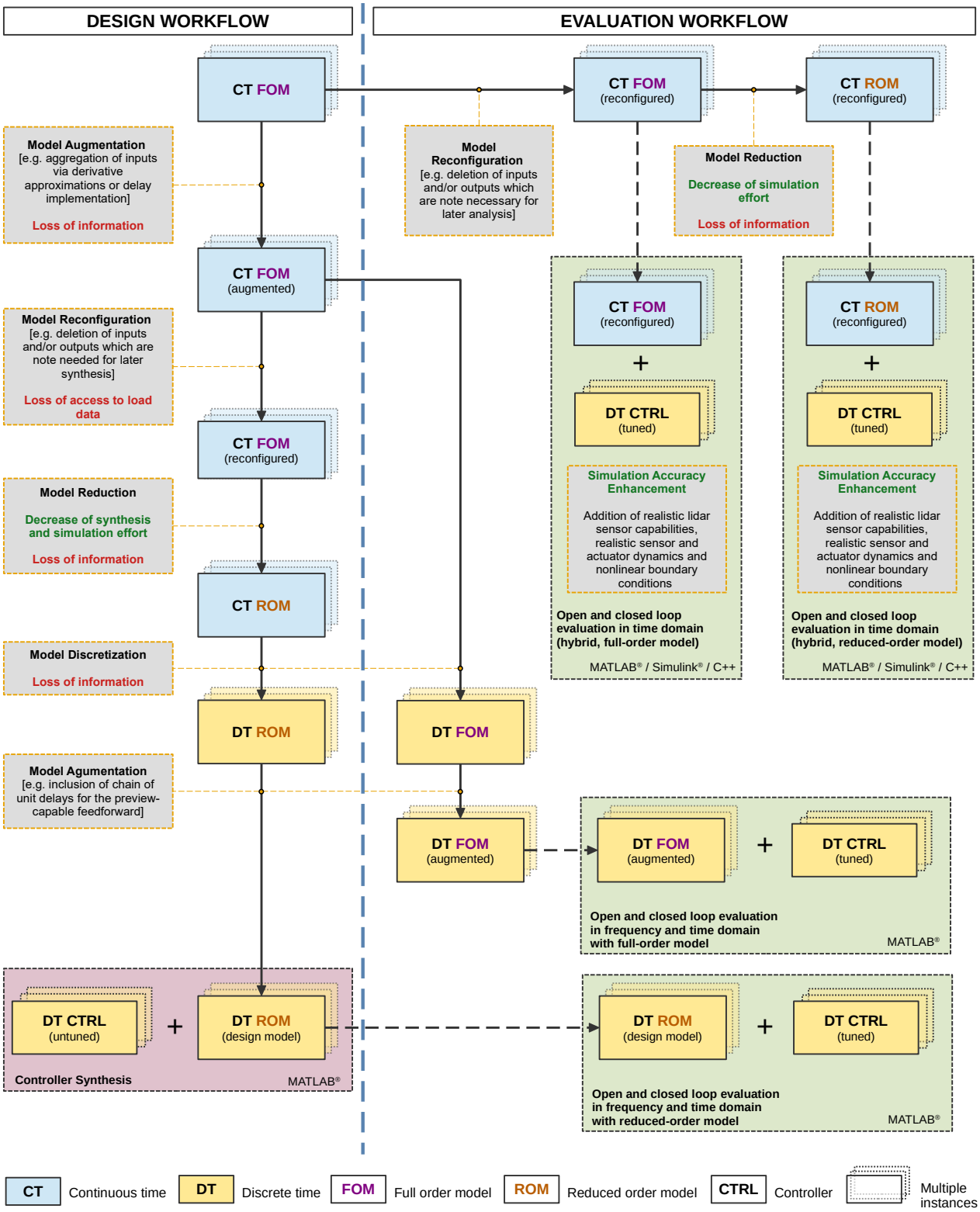

Figure 3 – Data/model flow during the design process (left side) and to obtain the different evaluation environments (right side, different levels of representativeness and computational cost)

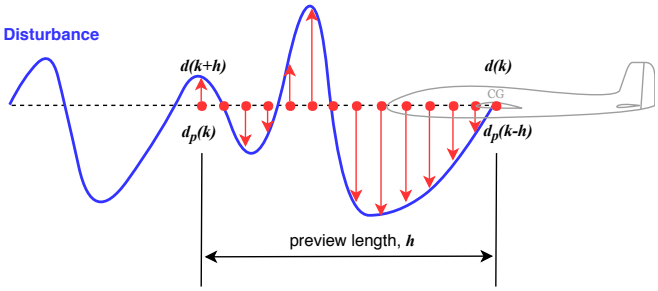

(a) Time-based discretization of an upcoming spatially distributed disturbance, aircraft is flying from right side to left side

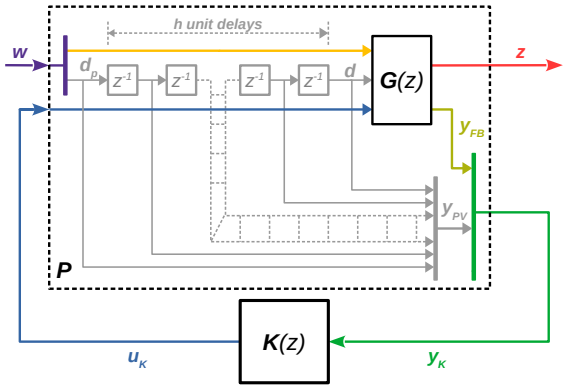

(b) Chain of unit delays (tapped delay line) and resulting additional sensor signals

Figure 4 – Discretized model augmentation via lidar sensor approximating unit delays

troller with the model it has been designed for (possibly removing some weighting functions used only for design): this case correspond to the validation at the lower right corner of the diagram. By moving upward various other combinations of models and controllers can be combined to create evaluation environments of varying level of representativeness. In a sense, the design workflow moving downward along the left side of the diagram shown Figure 3 and moving upward along the right side of this diagram may be compared to the two branches of the V-model for system development. Whilst this analogy is not nearly perfect, there are similar cross connections between the simplifications made in the design and the levels of validations that can be produced based on the intermediate models. If the validation fails when the controller is combined with one of the most simple models or directly the one used for designing it, there is very little chance that tests with the more complex models will be passed. The tests with the most simple models are still useful because they are cheaper[1] to perform and if they fail, the cause(s) is(are) usually easier to identify and understand.

4.2 Modular Hybrid and Multi-Rate Simulation Environment

Simulink® allows the integration and the coupling of various components (submodels) from different sources to model complex systems. The numerical solvers provided with Simulink® allow the simulation of continuous-time, discrete-time, and hybrid[2] systems (possibly nonlinear). Figure 5 shows the overall structure of the simulation environment built using Simulink®. The complete system is a hybrid and multi-rate system with the continuous-time components being represented by the light-blue blocks and the discrete-time components being represented with the other colors (each color representing a different rate).

To enhance the accuracy of the simulation, the Simulink®-based load evaluation is including generic nonlinear actuator models, implemented in continuous time, for each control surface except for the ailerons. The generic nonlinear actuator models are second-order systems with dynamically adjustable parameters (angular frequency, damping, gain) and with position, rate, and accelerations limits. These parameters can be adjusted: for each actuator independently, depending on the flight point, and asymmetrically (e.g. to account for the aerodynamic and inertial loads acting on the control surface). They are implemented as C++ S-functions.

In addition to the generic actuator approach, the evaluation environment is featuring specific actuator models for the ailerons, provided by Liebherr Aerospace, implemented as a S-function. These models are denoted by complex inner dynamics, based on real nonlinear kinematics (including limitations)

[1] On high-order systems (several thousand of states) and with many inputs and outputs, computing the frequency response may take several hours on a standard desktop computer, but be obtained in a few seconds for their reduced-order approximation.

[2] i.e. involving both continuous-time and discrete-time elements

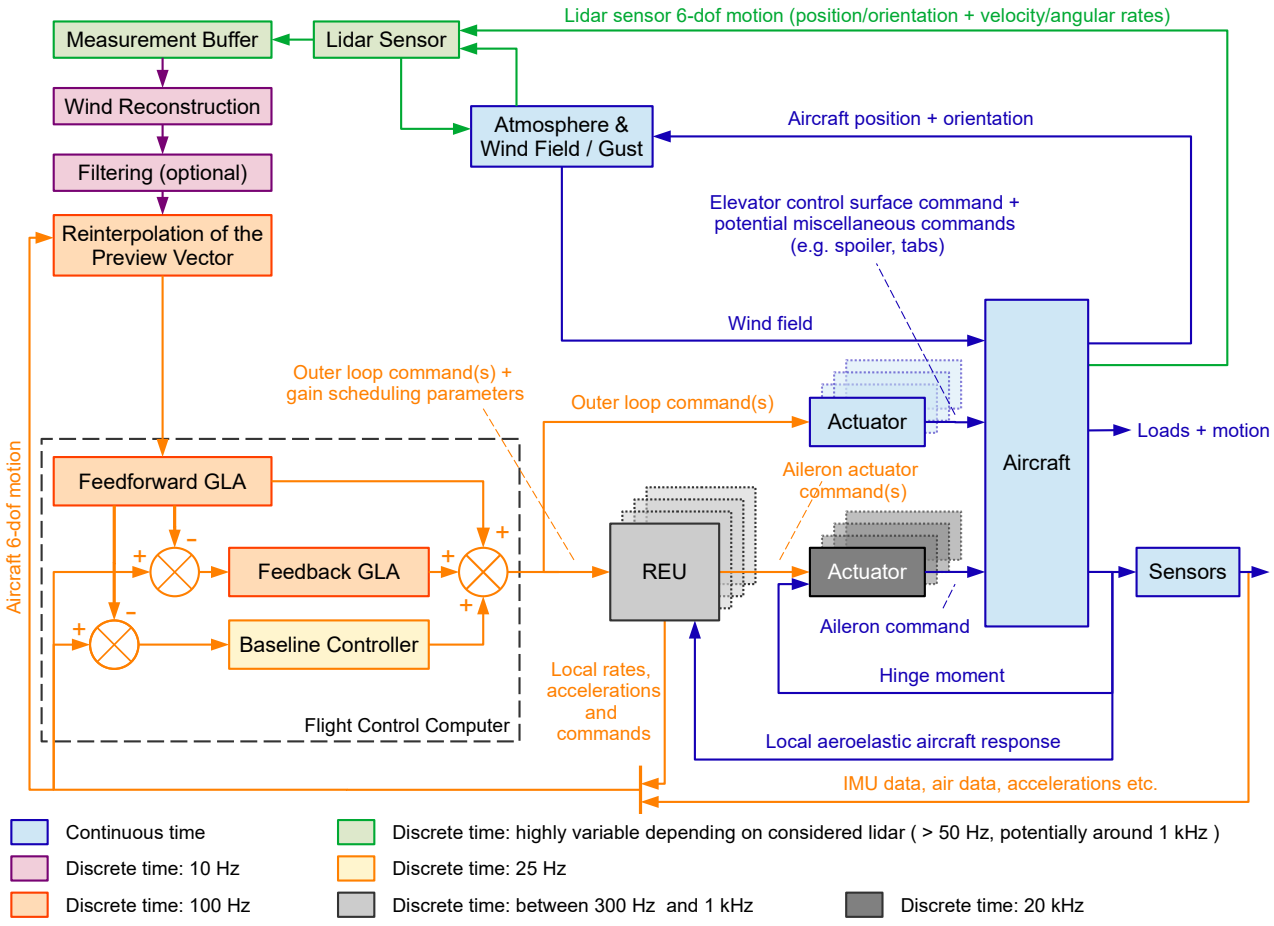

Figure 5 – Simulink®-based hybrid and multi-rate simulation environment including REU

and a very detailed powertrain modeling. Overall, a sampling frequency of 20 kHz is required. Each actuator model is featuring an input for the hinge moment to account for the current load acting on the actuator. In the considered controller architecture, the aileron actuators are supplemented by the Remote Electronic Units. REU are implemented in discrete time, running at a sampling frequency between 300 Hz and 1 kHz and implement the actuator control loop, the aforementioned fast inner loops. The outer-loop commands are computed and provided by the central flight control computer.

The lidar sensor model and the wind reconstruction algorithm (which allows the interpretation of the raw lidar measurements) are implemented in C++. Both elements are integrated in a single S-function to simplify the implementation, but running at individual rates. The sensor rate is possibly as large as 1 kHz and depends strongly on the lidar sensor configuration. The wind reconstruction algorithm ([8, 15, 33]) does not need to run as frequently as the feedforward gust load alleviation controller, thanks to the re-interpolation of the preview vector performed before sending the reconstructed wind to the feedforward GLA controller. This re-interpolation permits to account for the aircraft motion between two successive steps even if the reconstructed wind profile has not been updated. The lidar simulation model relies on a surrogate model, which is derived from a significantly more complex end-to-end lidar sensor simulation (cf. later Figure 6). The end-to-end lidar simulation considers the different processes from the laser emission, through the optics and the atmosphere, the backscattering of the laser light by the molecules of (and if present particles in) the air, and the detector. It allows the investigation of the influence of the different system parameters, but is computationally demanding and therefore not suited for coupling with the aeroservoelastic simulation. The surrogate model provides less options for the parametric investigations but is very cheap to compute while considering all major physical effects and therefore ideal for the aeroservoelastic simulations.

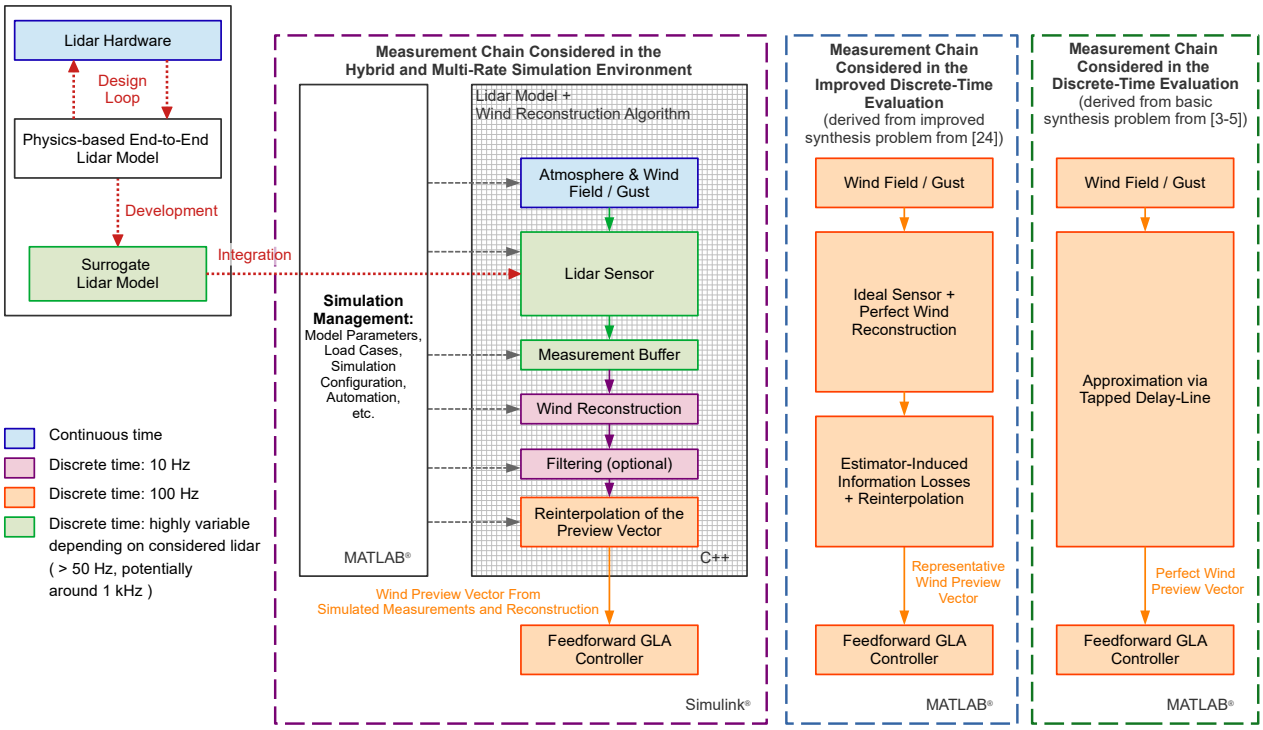

Figure 6 – Comparison between multi-rate and hybrid simulation and discrete time evaluation, regarding lidar sensing capability approximation

4.3 Understanding and Reducing the Differences between the Results from the Hybrid Multi-Rate Simulation and from the Other Evaluations

Additionally, differences in terms of sampling rate between the different systems are neglected in some of the various evaluation environments. As long as the effective bandwidths of designed control functions do not come close to the corresponding Nyquist frequency, the differences in terms of computed load levels can be expected to remain fairly small. Further differences could also result from using simplified linear actuator models, if nonlinearities (e.g. rate limits) were reached. Until now, combinations of simplified aeroelastic models with nonlinear actuator models have not been needed (and therefore developed), but such combinations can be considered as well. For fairly aggressive feedback control functions (i.e., lacking the anticipation time provided by the lidar sensor), the risk of reaching rate limits is higher and the added-value of such environment might be larger.

One of the core elements of the hybrid simulation environment is the lidar sensor simulation and the subsequent wind reconstruction algorithm. As schematically represented in the top-left corner of Figure 6, the central element of the lidar sensing is mainly composed of a numerically well-conditioned lidar sensor simulation model, called Surrogate Lidar Model. It is derived from its continuously refined and more detailed physics-based counterpart, the End-to-End Lidar Sensor Model. The physics-based end-to-end lidar sensor simulation itself is computationally too expensive for an utilization in a coupled simulation respectively for the controller development. The Surrogate Lidar Model reflects the main characteristics of the sensor, such as spatial resolution, blur, measurement errors (bias, noise, etc.).

4.4 Automation of Loads Evaluation for Multiple Combinations of Controller

The computation of the gust load envelope necessarily requires a large number of simulations. All combinations of flight point, mass case, as well as gust length and direction have to be considered. Depending on the considered aircraft configuration, the number of simulations rapidly grows and in the order of several thousands simulations are typically needed for each combination of control functions. Additionally, for systems engineering tasks, variations of other system parameters (e.g.,

lidar sensor parameters) need to be performed to assess their impact on the system performance. The automation of the load computation and, afterward, of the assessment of the results is of utmost importance.

Beyond the obvious parameter variations permitting to cover the entire range (or, if desired, a subset) of flight conditions, mass cases, gust lengths and the management of the corresponding computations (initialization and configuration of the simulations, retrieval and archiving of the results), the developed automatized load computation and assessment also provided high-level functionalities supporting systems engineering tasks. For instance, the overall decentralized flight control architecture presented above consists of several controllers and systems (e.g., lidar and REU) and different combinations of these systems (possible even considering several variants for each) can be defined and evaluated at once. The results can easily be compared to optimize the overall system.

In the case of the different control functions, the concept of "controller configurations" is defined and used. A controller configuration is defined as a combination of controller functions and their parameters (including gain-scheduling). A typical set of controller configurations that is worth considering in the framework of the INTELWI project reads:

- an open loop case (i.e., no controller active),
- a rigid-body law only case,
- a rigid-body law + feedforward gust load alleviation case,
- a rigid-body law + feedback gust load alleviation case,
- a rigid-body law + feedback and feedforward gust load alleviation case,
- any of the previous case combined with a decentralized controller running on the REU.

Several alternative designs or tuning of these controllers can be considered, for instance with more or less aggressive behaviors. A typical question that can easily be investigated, would be whether splitting one or two ailerons into more individual surfaces is advantageous: such aileron split yielding possibly higher load alleviation potential, but probably at the cost of higher system mass and complexity.

The automated evaluation also includes a load hierarchy feature with which, for each controller configuration and load type/station, a hierarchy of load cases is computed. During the design of the load alleviation system and especially during the fine tuning of the control functions, the provided worst-case loads for each load type and station is very valuable. The designer can better understand the options available and progress more quickly towards a good trade-off between the conflicting requirements.

5. Summary and Outlook

The MATLAB®- and Simulink®-based hybrid simulation environment eases to perform gust load evaluations for arbitrary controller configurations, i.e. combinations of control functions, designed with different synthesis methods or made for various control objectives. The investigated aircraft model can be very detailed and complex. Often, the aircraft dynamics are represented by a set of linear models. Each aircraft model can be augmented with realistic actuating and sensing capabilities, especially with an advanced lidar sensor model, providing the possibility to include highly representative simulations of the control system. Simulated configurations are extendable via arbitrary submodels, which can be implemented in discrete time (with various sampling rates) or in continuous time, and essential parts of the simulation are parametrized. This parametrization allows to change the test conditions as well as actuator and sensing capabilities dynamically and to switch very easily between different controller configurations to be investigated. The simulated load case data could be exploited via a detailed loads analysis tool, able to generate the load hierarchy for each load component and every load station. The load evaluation environment presented provides the necessary features to evaluate novel controller approaches including REU-based local feedback loops, lidar-based feedforward gust load alleviation functions, or a combination of both concepts. Its level of automation

eases systems engineering studies, trade-off analysis, as well as in-depth performance evaluations. The environment constitutes a tool which is developed on an as-needed basis by the authors: at the time of writing, no additional feature is planed for the near future, but in-depth load evaluations of the presented control approach will follow soon.

6. Contact Author Email Address

christian.wallace@dlr.de

7. Acknowledgment

This work is a collaboration between the German Aerospace Center (DLR) and Liebherr and is performed within the framework of the German national research project INTELWI (Förderkennzeichen 20A1903A).

8. Copyright Statement

References

[1] Pusch, M., Kier, T., Tang, M., Dillinger, J., and Ossmann, D., "Advanced gust load alleviation using dynamic control allocation," in *AIAA Scitech Forum 2022*, San Diego, CA, USA, Jan. 3–7, 2022. DOI: 10.2514/6.2022-0439.

[2] Fezans, N. and Joos, H.-D., "Combined feedback and LIDAR-based feedforward active load alleviation," in *Proceedings of the 2017 AIAA Aviation Forum*, AIAA 2017-3548, Denver, CO, USA, Jun. 5–9, 2017. DOI: 10.2514/6.2017-3548.

[3] Khalil, A. and Fezans, N., "Performance enhancement of gust load alleviation systems for flexible aircraft using H_∞ optimal control with preview," in *Proceedings of the 2019 AIAA SciTech Forum*, San Diego, CA, USA, Jan. 7–11, 2019. DOI: 10.2514/6.2019-0822.

[4] Khalil, A. and Fezans, N., "A multi-channel H_∞ preview control approach to load alleviation function design," in *Proceedings of the 5th CEAS Conference on Guidance, Navigation and Control (Euro GNC 2019)*, Milano, Italy, Apr. 3–5, 2019. [Online]. Available: https://elib.dlr.de/128625.

[5] Cavaliere, D., Fezans, N., Kiehn, D., Quero, D., and Vrancken, P., "Gust load control design challenge including lidar wind measurements and based on the common research model," in *AIAA Scitech 2022 Forum*, San Diego, CA, USA, Jan. 3–7, 2022. DOI: 10.2514/6.2022-1934.

[6] Weber, G. *et al.*, "Decentralized load alleviation system," in *SEE MEA (More Electric Aircraft)*, Bordeaux, France, Oct. 20–21, 2021. [Online]. Available: https://elib.dlr.de/146762.

[7] Fezans, N., Vrancken, P., Linsmayer, P., Wallace, C., and Deiler, C., "Designing and maturating doppler lidar sensors for gust load alleviation: Progress made since AWIATOR," in *Proceedings of the Aerospace Europe Conference*, Bordeaux, France: CEAS / 3AF, Feb. 25–28, 2020. [Online]. Available: https://elib.dlr.de/134227.

[8] Kiehn, D., Fezans, N., Vrancken, P., and Deiler, C., "Parameter analysis of a doppler lidar sensor for gust detection and load alleviation," in *The International Forum on Aeroelasticity and Structural Dynamics (IFASD)*, IFASD-2022-105, Madrid, Spain, Jun. 13–17, 2022.

[9] Fezans, N., Wallace, C., Kiehn, D., Cavaliere, D., and Vrancken, P., "Lidar-based gust load alleviation - results obtained on the Clean Sky 2 Load Alleviation Benchmark," in *The International Forum on Aeroelasticity and Structural Dynamics (IFASD)*, IFASD-2022-155, Madrid, Spain, Jun. 13–17, 2022.

[10] Jenaro Rabadan, G., Schmitt, N. P., Pistner, T., and Rehm, W., "Airborne lidar for automatic feedforward control of turbulent in-flight phenomena," *Journal of Aircraft*, vol. 47, no. 2, pp. 392–403, 2010. DOI: 10.2514/1.44950.

[11] Cézard, N., Besson, C., Dolfi-Bouteyre, A., and Lombard, L., "Airflow characterization by Rayleigh-Mie lidars," *AerospaceLab*, no. 1, pp. 1–4, 2009. [Online]. Available: https://aerospacelab.onera.fr/al1/Airflow-characterization-by-Rayleigh-Mie-lidars.

[12] Herbst, J. and Vrancken, P., "Design of a monolithic Michelson interferometer for fringe imaging in a near-field, UV, direct-detection Doppler wind lidar," *Applied Optics*, vol. 55, no. 25, pp. 6910–6929, 2016. DOI: 10.1364/AO.55.006910.

[13] Vrancken, P. and Herbst, J., "Development and Test of a Fringe-Imaging Direct-Detection Doppler Wind Lidar for Aeronautics," in *EPJ Web of Conferences, 29th International Laser Radar Conference*, Hefei, People's Republic of China, Jun. 24–28, 2019. [Online]. Available: https://elib.dlr.de/123605.

[14] Vrancken, P. and Herbst, J., "A Novel Direct-Detection Doppler Wind Lidar Based on a Fringe-Imaging Michelson Interferometer as Spectral Analyzer," in *2nd European Lidar Conference*, Granada, Spain (virtual), Nov. 18–19, 2020. [Online]. Available: https://elib.dlr.de/138976.

[15] Fezans, N., Joos, H.-D., and Deiler, C., "Gust load alleviation for a long-range aircraft with and without anticipation," *CEAS Aeronautical Journal*, vol. 10, pp. 1033–1057, 2019. DOI: 10.1007/s13272-019-00362-9.

[16] Khalil, A. and Fezans, N., "Gust load alleviation for flexible aircraft using discrete-time H_∞ preview control," *The Aeronautical Journal*, vol. 125, no. 1284, pp. 341–364, 2021. DOI: 10.1017/aer.2020.85.

[17] Khalil, A. and Fezans, N., "A multi-channel H_∞ preview control approach to load alleviation design for flexible aircraft," *CEAS Aeronautical Journal*, vol. 12, pp. 401–412, 2021. DOI: 10.1007/s13272-021-00503-z.

[18] Hofstee, J., Kier, T., Cerulli, C., and Looye, G., "A variable, fully flexible dynamic response tool for special investigations (varloads)," in *International Forum on Aeroelasticity and Structural Dynamics (IFASD)*, Amsterdam, Netherlands, Jun. 4–6, 2003. [Online]. Available: https://elib.dlr.de/12206.

[19] Schulz, S., Ossmann, D., Milz, D., Kier, T., and Looye, G., "Aircraft mission simulation framework for loads analysis," in *AIAA Scitech 2020 Forum*, Orlando, Florida, USA, Jan. 6–10, 2020. DOI: 10.2514/6.2020-1620.

[20] Wuestenhagen, M., "Synthesis of a multiple-model adaptive gust load alleviation controller for a flexible flutter demonstrator," in *AIAA Scitech 2022 Forum*, San Diego, CA, USA, Jan. 3–7, 2022. DOI: 10.2514/6.2022-0440.

[21] Weiser, C. and Ossmann, D., "Baseline flight control system for high altitude long endurance aircraft," in *AIAA Scitech 2022 Forum*, San Diego, CA, USA, Jan. 3–7, 2022. DOI: 10.2514/6.2022-1390.

[22] Kier, T., "An integrated loads analysis model for wake vortex encounters," in *International Forum on Aeroelasticity and Structural Dynamics (IFASD)*, Bristol, UK, Jun. 24–26, 2013. [Online]. Available: https://elib.dlr.de/97799.

[23] Kier, T., Müller, R., and Looye, G., "An integrated analysis model for assessment of critical load conditions for the vertical tail plane," in *International Forum on Aeroelasticity and Structural Dynamics (IFASD)*, Savannah, GA, USA, Jun. 10–13, 2019.

[24] Guyan, R. J., "Reduction of stiffness and mass matrices," *AIAA Journal*, vol. 3, no. 2, p. 380, 1965. DOI: 10.2514/3.2874.

[25] *Certification specifications and acceptable means of compliance for large aeroplanes (cs-25) - amendment 27*, European Union Aviation Safety Agency (EASA), Nov. 24, 2021.

[26] Waszak, M. R. and Schmidt, D. K., "Flight dynamics of aeroelastic vehicles," *Journal of Aircraft*, vol. 25, no. 6, pp. 563–571, 1988. DOI: 10.2514/3.45623.

[27] Bisplinghoff, R. L., Ashley, H., and Halfman, R. L., *Aeroelasticity*. Dover Publications Inc., 1955.

[28] Kier, T. and Looye, G., "Unifying manoeuvre and gust loads analysis," in *International Forum on Aeroelasticity and Structural Dynamics (IFASD)*, Seattle, Washington, USA, Jun. 21–25, 2009. [Online]. Available: https://elib.dlr.de/97798.

[29] Sutherland, J., "Fly-by-wire flight control systems," Air Force Flight Dynamics Laboratory (FDGL), Wright-Patterson Air Force Base, Ohio, USA, Technical Report, Sep. 1968, AD 679 158.

[30] Niedermeier, D. and Lambregts, A., "Fly-by-wire augmented manual control - basic design considerations," in *28th International Congress of the Aeronautical Sciences (ICAS)*, Brisbane, Australia, Sep. 23–28, 2012. [Online]. Available: https://www.icas.org/ICAS_ARCHIVE/ICAS2012/PAPERS/605.PDF.

[31] Cavaliere, D., Fezans, N., and Kiehn, D., "Method to account for estimator-induced previewed information losses - application to synthesis of lidar-based gust load alleviation functions," in *CEAS EuroGNC 2022 - Conference on Guidance, Navigation and Control*, Berlin, Germany, May. 3–5, 2022.

[32] Padé, H., "Sur la représentation approchée d'une fonction par des fractions rationelles," *Annales Scientifiques de L'É.N.S.*, vol. 9, pp. 3–93, 1892.

[33] Fezans, N., Schwithal, J., and Fischenberg, D., "In-flight remote sensing and identification of gust, turbulence, and wake vortices using a Doppler LIDAR," *CEAS Aeronautical Journal*, vol. 8, no. 2, pp. 313–333, 2017. DOI: 10.1007/s13272-017-0240-9.